JOURNAL OF GEOPHYSICAL RESEARCH, VOL. 106, NO. B12, PAGES 30,835–30,848, DECEMBER 10, 2001

Crustal structure and thermal anomalies of the Dunedin Region, South Island, New Zealand

Nicola J. Godfrey,[1,2] Fred Davey,[3] Tim A. Stern,[4] and David Okaya[1]

Abstract. Seven geophysical data sets are used to investigate a transect along the southeast coast of South Island, New Zealand. The specific focus of this study is the Dunedin volcanic center, which last produced volcanics at the surface 13–10 Myr ago. Wide-angle reflection/refraction seismic data along a two-dimensional profile reveal a low-velocity lower crust and mantle beneath the Dunedin volcanic center. The low-velocity lower crust coincides with a highly reflective region on a nearby multichannel seismic line and may represent a hot, fluid-rich region of the crust. In addition, high mantle helium ratios measured in the Dunedin region suggest a current or recent mantle-melting event. High heat flow recorded in the Dunedin region is consistent with a hot body emplaced in the midcrust ~10 Myr ago (Miocene) whose heat is just reaching the surface today. Uplift of an Oligocene limestone horizon in the Canterbury basin can be explained by a buoyant load beneath the Dunedin volcanic center and low flexural rigidity of the lithosphere beneath the volcanic center during the Miocene. We interpret the data as revealing two separate thermal events beneath the Dunedin volcanic center, one during the Miocene, when volcanism was last occurring at the surface, and the other occurring currently. Active volcanism associated with the current mantle-melting event has yet to reach the surface.

1. Introduction

The Dunedin and Banks Peninsula volcanic centers are conspicuous landforms on the southeast coast of South Island, New Zealand (Figure 1a). They were active during the Miocene, producing a combined total of ~2000 km^3 of erupted basalts. The last volcanic activity was ~10 Myr ago at the surface in the Dunedin region and ~5.8 Myr ago on the Banks Peninsula [*Coombs et al*., 1986; *Coombs*, 1987; *Hoke et al*., 2000]. More recently (~2.5 Ma) volcanics were erupted near Timaru [*Duggan and Reay*, 1986] (Figure 1b). The volcanic centers on South Island are of uncertain origin. They are intraplate volcanoes that do not appear to be related to a mantle plume but that are presumed to be too far behind the active plate margin to be subduction related [*Hoke et al*., 2000].

Heat flow data (Figure 1b) show anomalously high values in the Dunedin region (~90 mW m^{-2}, compared with the background value for South Island of ~60 mW m^{-2}) and are most likely related to the Miocene volcanism [*Funnell and Allis*, 1996; *Cook et al*., 1999]. In addition, high percentages (>80%) of mantle helium (Figure 1b) have been recorded in the Dunedin region and smaller (25%), but significant percentages of mantle helium have been recorded on the Banks Peninsula [*Giggenbach et al*., 1993; *Hoke and Sutherland*, 1999; *Hoke et al*., 2000]. Such high levels of mantle helium are indicative of active melting and basaltic addition to the crust [*O'Nions and Oxburgh*, 1983], despite the lack of volcanic activity at the surface today.

In 1996 the South Island GeopHysical Transect (SIGHT) experiment set out to record two onshore-offshore wide angle-reflection/refraction (WAR/R) transects across the width of South Island [*Stern et al*., 1997; *Davey et al*., 1998]. Offshore multichannel seismic (MCS) data were collected as part of these transects (Figure 1a), and an additional MCS transect was planned along the southeast coast of South Island. The scheduling of the field experiment enabled some of the onshore instruments from the main transects to be re-deployed along a third transect, Transect 3, to record air gun shots from the MCS profiles along the southeast coast of South Island (Figure 1a). The combination of velocities derived from the wide-angle reflection/refraction (WAR/R) data and reflection images from the multichannel seismic data provides important new information about the crust and mantle beneath the Dunedin volcanic center that can be related to the preexisting helium isotope and heat flow data. In addition, the velocity model and MCS images provide new constraints on the subsurface geometry of the accretionary terranes that make up the southeast part of South Island (also see N. Mortimer et al., Crustal structure across an extended Phanerozoic convergent margin: Eastern Province and Median Batholith of New Zealand, submitted to *New Zealand Journal of Geology and Geophysics*, 2001, hereinafter referred to as Mortimer et al., submitted manuscript, 2001).

2. Tectonic and Geologic Setting

2.1. Tectonic Setting

From Permian to Cretaceous times a subduction zone existed along the Pacific sector of the Gondwana margin [*Bishop et al*., 1985; *Rattenbury*, 1987], which resulted in subduction-related arc magmatism [*Gibson and Ireland*, 1995] and the accretion of the Eastern Province terranes [*Norris et al*., 1990;

[1]Department of Earth Sciences, University of Southern California, Los Angeles, California, USA.
[2]Now at Landmark EAME, Weybridge, England, UK.
[3]Institute of Geological and Nuclear Sciences, Lower Hutt, New Zealand.
[4]Research School of Earth Sciences, Victoria University, Wellington, New Zealand.

Paper number 2000JB000006.
0148-0227/01/2000JB000006$09.00

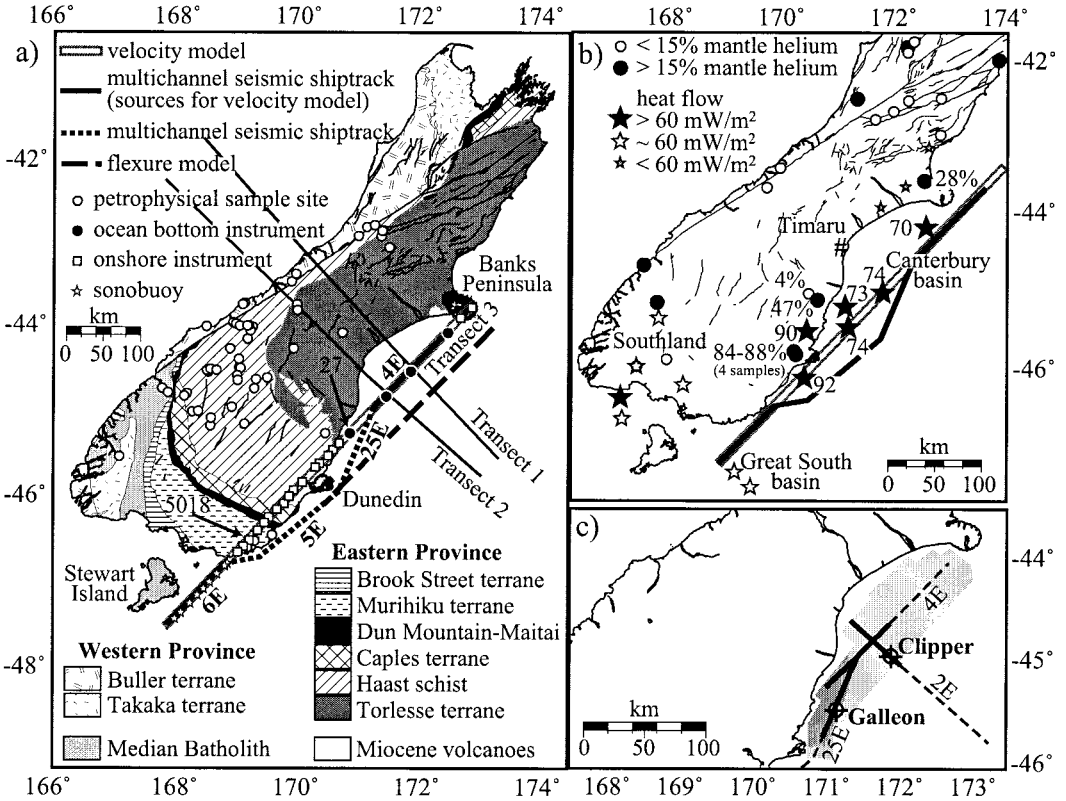

Figure 1. (a) Terrane map of South Island, New Zealand, showing major faults, geophysical profiles discussed in the text, and the locations of seismic recorders and petrophysical sample sites. (b) Heat flow (stars) and helium isotope (circles) measurements on South Island (values given for sites close to Transect 3). (c) Enlargement showing additional SIGHT multichannel seismic lines and industry wells used. Sections of seismic lines shown with solid lines are shown in Figure 5. Light shaded region shows coverage of dense grid of industry multichannel seismic lines [*B.P. Shell Todd*, 1982; *Field and Browne*, 1989]. Dark shaded region is portion of industry data set that shows the uplifted section of the Oligocene horizon near Dunedin discussed in the text.

Davey et al., 1998]. By 110 Ma (early Cretaceous), plate convergence had essentially ceased and was followed by the extensional collapse of the magmatically thickened and thermally weakened continental arc [*Gibson and Ireland*, 1995].

Two episodes of rifting occurred during the mid-Cretaceous and early Late Cretaceous, the latter separating New Zealand from Australia and Antarctica [*Bishop and Turnbull*, 1996]. At 60 Ma (Paleocene), seafloor spreading within the Tasman Sea was replaced by rifting perpendicular to the earlier spreading direction, along the southwest margin of the Tasman Sea, and between New Zealand and Australia and Antarctica. Spreading continued until about 30 Ma (Oligocene), when a small amount of relative motion that had developed between the Pacific and Australian plates became more oblique [*Wood and Sutherland*, 1997]. The Alpine fault, the surface trace of the Pacific-Australian plate boundary through southern New Zealand, developed as a through-going strike-slip plate boundary at about 25 Ma [*Molnar et al*., 1975; *Carter and Norris*, 1976; *Cooper et al*., 1987]. A change in the relative plate motion along the Pacific-Indian plate boundary ~10 Myr ago [*Molnar et al*., 1975; *Carter and Norris*, 1976] resulted in increasingly oblique motion on the Alpine fault. Substantial shortening (50–100 km) has occurred perpendicular to the fault over the last 10 Myr [*Molnar et al*., 1975; *Walcott*, 1979; *Allis*, 1981; *Walcott*, 1984], with compression increasing markedly since 5 Ma [*Walcott*, 1979; *Wood and Sutherland*, 1997; *Walcott*, 1998].

2.2. Geologic Setting

Transect 3 crosses the Eastern Province, the Median batholith, and the Miocene volcanic centers of Dunedin and the Banks Peninsula (Figure 1a). A number of Permian to Jurassic tectonostratigraphic terranes were accreted during the Mesozoic to form the Eastern Province [*Norris et al*., 1990; *Davey et al*., 1998]. These terranes trend southeast onshore and continue offshore beneath the Cretaceous-Cenozoic Great South basin [*Bishop and Turnbull*, 1996] (Figures 1a and 1b). From southwest to northeast, they include the Permo-Jurassic arc and forearc basin system of the New Zealand region (the Brook Street (volcanoplutonic arc), Murihiku (forearc basin), and Dun Mountain-Maitai (oceanic affinity) terranes) and the coeval relatively mafic volcanoclastic Caples and quartzo-feldspathic Torlesse accretionary terranes (Figure 1a). See Appendix A for more detail about the Eastern Province terranes. The collision of the Caples and Torlesse accretionary terranes during the Early Cretaceous Rangitata Orogeny (120–150 Ma) resulted in the formation of the Haast Schist [*Coombs et al*., 1976; *Bishop et al*., 1985; *Mortimer*, 1993a, 1993b] (Figure 1a).

The Median batholith is part of a Carboniferous-Cretaceous Andean-type arc that intruded the Western Province Takaka terrane and the Eastern Province Brook Street terrane [*Mor-*

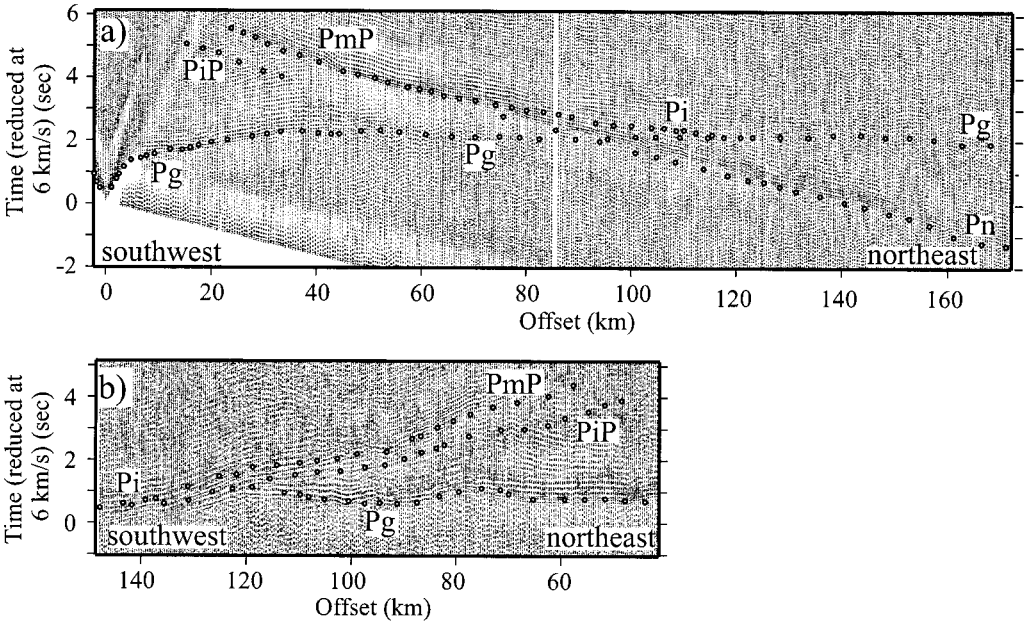

Figure 2. Wide-angle reflection/refraction seismic data recorded along Transect 3. Circles show arrival times of model phases. (a) Gather recorded by ocean bottom instrument 27 (see Figure 1a for location). Sources are air gun shots from SIGHT line 4E. (b) Gather recorded by onshore station 5018 (see Figure 1a for location). Sources are air gun shots from SIGHT line 6E.

timer et al., 1999] during late Jurassic and Cretaceous times, in response to subduction at the Gondwana margin [*Bishop et al*., 1985; *Rattenbury*, 1987].

The Dunedin Volcanic Group includes the intraplate basalts of the Dunedin region and Banks Peninsula as well as other smaller volcanic centers on South Island, which were active during the middle Miocene. Activity at the Dunedin volcanic center began at 21 Ma, while the main volcano was constructed intermittently between 13 and 10 Ma [*Coombs et al*., 1986; *Coombs*, 1987]. A 20-mGal amplitude, 20-km-wide gravity anomaly over the volcano has been modeled as a cylindrical magma chamber that is partially full of high-density olivine gabbro [*Reilly*, 1972]. Mantle xenolith flows are restricted to the edge of the volcano, suggesting the presence of a major magma chamber, which hindered the ascent of xenolith flows to the surface [*Hoke et al*., 2000]. Ninety-five percent of the Dunedin volcanic center is alkali basalt, and geochemical data suggest that most of the lavas were mantle derived and underwent fractional differentiation in upper mantle magma chambers [*Bishop and Turnbull*, 1996].

The volcanoes on the Banks Peninsula formed between 11 and 5.8 Ma in four main eruptive phases. Volumetrically, the Banks Peninsula is the largest Miocene volcanic center on South Island, although production rates were low compared to typical hot spot driven volcanic activity [*Watson and McKenzie*, 1991].

3. Geophysical Data and Models

Data used to develop and constrain models presented here are WAR/R seismic data, MCS data from industry and the SIGHT program, petrophysical measurements, and helium isotope and heat flow data.

3.1. Wide-Angle Reflection/Refraction Seismic Data and Associated Velocity Model

3.1.1. Data. The 600-km-long, two-dimensional (2-D) velocity model described here is based on a subset of the Transect 3 WAR/R data. The entire Transect 3 WAR/R data set is too sparse to adequately constrain a true 3-D model. Only in-line shots and receivers were used to produce our 2-D model. The sources were air gun shots from SIGHT line 4E and the section of SIGHT line 6E that is collinear with line 4E (solid line, Figure 1a). These shots were recorded by four ocean bottom hydrophones (OBH) beneath SIGHT line 4E, 18 onshore Refraction Technology (REFTEK) recorders collinear with SIGHT line 4E (two of which are on the Banks Peninsula), and nine sonobuoys deployed along SIGHT line 6E (Figure 1a).

The station spacing is relatively coarse: 10–15 km spacing for onshore stations and 50–70 km spacing for ocean bottom instruments. The air gun shots had a shot interval of 50 m and a total air gun volume of 8495 cubic inches. No land sources were used for Transect 3.

Data quality is generally excellent (Figure 2). We were able to correlate crustal refractions (Pg), mantle refractions (Pn), Moho reflections (PmP), and a lower crustal reflection (PiP) between gathers. A lower crustal refraction (Pi) associated with the lower crustal reflection, PiP, was identified as a secondary arrival on most gathers (Figure 2). The sonobuoys recorded shallow upper crustal refractions (Pg) which helped constrain the near-surface velocities beneath SIGHT line 6E. The travel times of all identified phases were picked for incorporation into the velocity model.

3.1.2. Velocity model. Upper and midcrustal portions of the crust are modeled as a single layer with laterally and vertically variable velocities (dashed contour lines, Plate 1a). The

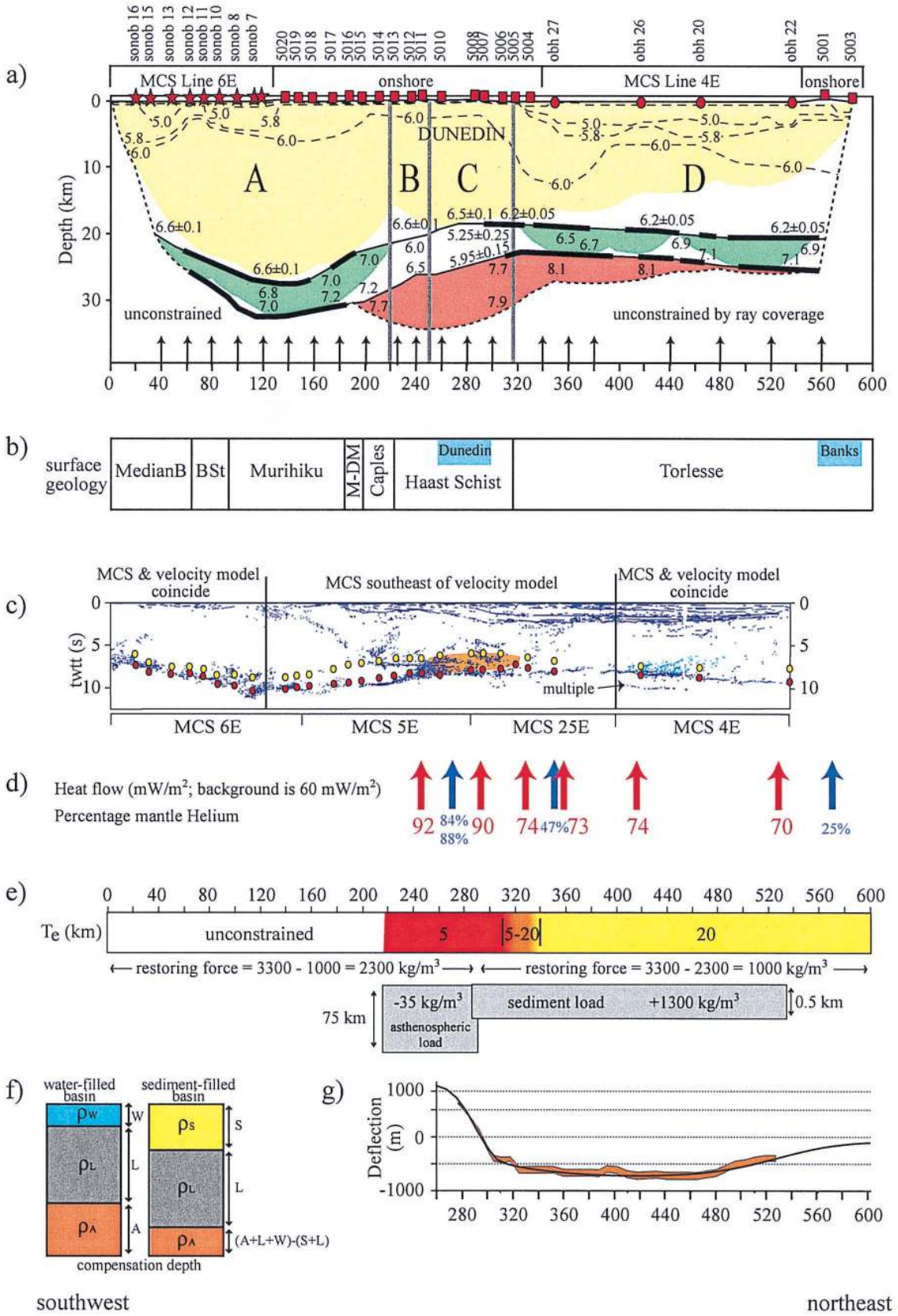
a)
sonob 16
sonob 15
sonob 13
sonob 12
sonob 11
sonob 10
sonob 8
sonob 7
5020
5019
5018
5017
5016
5015
5014
5013
5012
5011
5010
5008
5007
5006
5005
5004
obh 27
obh 26
obh 20
obh 22
5001
5003
MCS Line 6E
onshore
MCS Line 4E
onshore
DUNEDIN
A
B
C
D
Depth (km)
unconstrained
unconstrained by ray coverage
b)
surface geology
MedianB
BSt
Murihiku
M-DM
Caples
Haast Schist
Dunedin
Torlesse
Banks
c)
MCS & velocity model coincide
MCS southeast of velocity model
MCS & velocity model coincide
twtt (s)
multiple
MCS 6E
MCS 5E
MCS 25E
MCS 4E
d)
Heat flow (mW/m²; background is 60 mW/m²)
Percentage mantle Helium
92
84%
88%
90
74
47%
73
74
70
25%
e)
Te (km)
unconstrained
5
5-20
20
← restoring force = 3300 - 1000 = 2300 kg/m³ →
← restoring force = 3300 - 2300 = 1000 kg/m³ →
75 km
-35 kg/m³
asthenospheric load
sediment load
+1300 kg/m³
0.5 km
f)
water-filled basin
sediment-filled basin
ρw
ρL
ρA
ρs
W
L
A
S
(A+L+W)-(S+L)
compensation depth
g)
Deflection (m)
1000
0
-1000
southwest
northeast

lower crust is a separate layer whose top surface is constrained by wide-angle reflections (*PiP*), and whose velocity is constrained by the *Pi* phase. The third layer is the upper mantle (velocity constrained by *Pn*), whose top surface (Moho) is constrained by *PmP* reflections. Uncertainties in velocities shown in Plate 1a are based on perturbating the preferred velocity values until the misfit becomes intolerable (larger than the uncertainty in the travel time picks). Uncertainties so derived are in the range 1–5%. Boundary depths, where constrained by reflection bounce points, are accurate within ±0.5–1 km.

The most striking feature of our velocity model is the low-velocity (5.2–5.9 km s^{-1}) region in the lower crust beneath Dunedin (region C, Plate 1a). This overlies a low-velocity (7.7–7.9 km s^{-1}) region in the mantle (Plate 1a). Crustal velocities are generally lower to the north of Dunedin than to the south (Plate 1a).

Tests were made to see if the low velocities distributed between the lower crust and mantle can be placed either entirely above or below the Moho. If the low velocities are entirely in the lower crust, the *Pn* phase reduced at the "normal" mantle velocity (~8.1 km s^{-1}) will be horizontal on the travel time versus offset plot, and *Pn*, which travels through low-velocity lower crust, will be delayed compared to *Pn* traveling through normal velocity lower crust on either side. If the low velocities are entirely in the mantle, the *Pn* phase will become horizontal with an offset where the low-velocity mantle occurs for an apparent velocity <8.1 km s^{-1}. If the low velocities are distributed between the lower crust and mantle, a combination of these effects will be observed.

On gathers 5017 and 5019 (Plate 1) (recording shots from MCS line 4E), *Pn* passes through relatively fast lower crust (6.8–7.2 km s^{-1}) and enters the mantle in the low-velocity region. On a travel time plot reduced at 7.8–7.9 km s^{-1}, *Pn* is mostly horizontal with a slight kink where *Pn* travels through transitional-velocity mantle (Figures 3a and 3b). On gather OBH 27, however, the *Pn* phase, which also passes through relatively fast lower crust (6.5–6.7 km s^{-1}), can be flattened using an apparent velocity of ~8.1 km s^{-1} (Figure 3c). *Pn* on gather 5008 can also be flattened using an apparent velocity of ~8.1 km s^{-1} but arrives 0.5 s later than *Pn* on OBS 27 after passing through low-velocity lower crust (Figure 3c). The low-velocity zone is therefore distributed between the lower crust and mantle. The low velocities in the mantle are constrained by *Pn*, but no rays turn in the lower crustal low-velocity zone, so exact lower crustal velocities are poorly constrained. If the lower crust beneath Dunedin (region C, Plate 1a) has a velocity varying from 6.0 (top) to 6.4 (bottom) km/s, the modeled *Pn* arrives significantly early compared with the data. Within picking errors, two end-member velocity models for the lower crust have velocities of 5.5–6.1 and 5.0–5.8 km s^{-1} beneath Dunedin. We choose a velocity of 5.25 ± 0.25 km s^{-1} at the top and 5.95 ± 0.15 km s^{-1} at the bottom for the lower crust in region C (Plate 1a).

3.2. SIGHT MCS Data

Four SIGHT MCS lines along the southeast coast of South Island together form a ~600-km-long image of the crust beneath Transect 3. These data are discussed and interpreted in detail by Mortimer et al. (submitted manuscript, 2001). For the discussions in this paper we focus on the highly reflective lower crust beneath Dunedin and the Canterbury Basin (Plate 1c and Figure 4b).

3.2.1. Deep SIGHT MCS data. Zero-offset two-way travel times (TWTT) to the top of the lower crust and Moho in our WAR/R-derived velocity model are calculated and superimposed on the travel times of the MCS image (Plate 1c). The Moho in the velocity model coincides with the base of reflectivity on coincident MCS line 6E. Despite a 40-km gap between the MCS profile and the WAR/R profile, it is also close to the base of reflectivity interpreted as the Moho between model coordinates 120 and 400 (Plate 1c). Between model coordinates 400 and 540 the Moho in the velocity model (defined by *PmP*) is coincident with the reflector interpreted as the Moho on coincident MCS line 4E (Plate 1c).

The top of the lower crust in the velocity model is deter-

Plate 1. (opposite) (a) Velocity model. Numbers are velocities in km/s. Dashed lines are velocity contours. Dotted line shows extent of ray coverage (white areas have no ray coverage). Solid lines are velocity discontinuities (bold lines show locations of reflection bounce points). Shaded areas show regions sampled by refraction rays (yellow is upper crust, green is lower crust, and orange is mantle). Instrument locations are shown along the top of the model; stars are sonobuoys, squares are onshore stations, and solid circles are ocean bottom instruments. Vertical arrows at the base of the model show the locations of velocity-depth profiles. Thick vertical lines define regions (A through D) which are referred to in the text. (b) Mapped geology at the surface. Median B is the Median batholith, BSt is the Brook Street terrane, M-DM is the Maitai-Dun Mountain terrane, and Banks is the Banks Peninsula. Blue boxes show the location of the Miocene Banks Peninsula and Dunedin volcanic centers. (c) Line drawing of a multichannel seismic line partially coincident with the Transect 3 velocity model. The zero-offset two-way travel time (TWTT) to the top of the lower crust and Moho calculated from the velocity model are shown by yellow and red circles, respectively. The orange region marks the location of the low-velocity lower crust in the velocity model. (d) Locations of helium isotope (blue arrows) and heat flow (red arrows) measurements close to Transect 3 projected onto our model coordinate system. (e) Flexure model parameters. Upper section shows elastic thickness (T_e). Colored areas show the extent of the modeled weak elastic plate. The lower section shows the applied loads (a negative load is a buoyant load). (f) Schematic showing the mass balance used to determine the water-filled basin thickness (W) equivalent to a sediment-filled basin of thickness (S). L is lithosphere, A is asthenosphere, and ρ is density. (g) Flexural modeling results. Orange region represents data, and solid line is the model. The sediment load is 1300 kg m^{-3} (water with a density of 1000 kg m^{-3} replaced by sediments with a density of 2300 kg m^{-3}). The restoring force beneath the basin is 1000 kg m^{-3} (mantle with a density of 3300 kg m^{-3} replacing sediments with a density of 2300 kg m^{-3}). The restoring force beneath Dunedin is 2300 kg m^{-3} (mantle replacing water with no sediment loading). Modeling is based on a finite difference code for 2-D flexure of an elastic plate, where elastic thickness, loading, and restoring force can vary in an arbitrary manner [*Stern and ten Brink*, 1989].

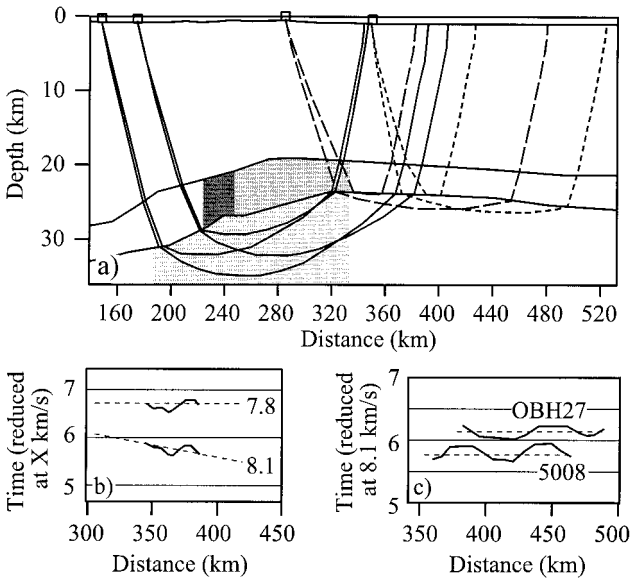

Figure 3. (a) Ray diagram for *Pn* phase recorded at four receiver locations (from left to right, 5019 (solid lines), 5017 (solid lines), 5008 (dashed lines), and OBH27 (dotted lines). Only minimum and maximum offset rays are shown. Shaded regions are the low-velocity zones shown in Plate 1a. (b) *Pn* arrival times taken from the data for receiver 5019 shown with reduction velocities of 7.8 and 8.1 km/s. (c) *Pn* arrivals time taken from the data for receivers 5008 and OBH27 shown with a reduction velocity of 8.1 km/s.

mined from wide-angle reflections (*PiP*) everywhere except in the Dunedin region. Between model coordinates 40 and 120, the top of lower crust in the velocity model is approximately coincident with the top of a reflective region in the lower crust (Plate 1c). The onset of reflectivity in the lower crust in this region is associated with an impedance contrast sampled by the wide-angle reflections. Beneath Dunedin (model coordinates 250–320) the top of the lower crust, which is not defined by wide-angle reflections but which marks a velocity inversion, is approximately coincident with the top of a highly reflective lower crustal section (Plate 1c) (although the velocity model and MCS line are up to 40 km apart in this region).

3.2.2. Shallow SIGHT MCS data. Within the Canterbury basin, at the northeast end of Transect 3, SIGHT lines 4E and 25E both show a prominent reflector that is most likely the Oligocene limestone horizon that is ubiquitous on offshore seismic data from New Zealand (solid line, Figures 5a and 5c) [*Holt and Stern*, 1994]. As SIGHT lines 4E and 25E approach Dunedin, this reflector is uplifted, and on SIGHT line 25E it is truncated at the surface (Figure 5c). It was presumably deposited horizontally, which makes it a useful marker horizon whose profile can be used to calibrate uplift. The age of uplift can be estimated from the age of the shallowest uplifted horizon on which there are onlapping sediments as seen on SIGHT line 4E (Figure 5a).

3.3. Industry Well Data

Two industry wells either on, or close to, three of the SIGHT MCS lines (Figure 1c) are used to date the horizon that we expect to be the Oligocene limestone and the shallowest uplifted horizon. We mapped both horizons from SIGHT line 4E to SIGHT lines 2E and 25E (Figure 5). On SIGHT lines 25E and 2E the deeper prominent reflector ties with the Oligocene limestone horizon in the well logs of the Galleon-1 well (Figures 1c and 5c and Table 1) [*Wilson*, 1985] and the Clipper-1 well (Figures 1c and 5b and Table 1) [*Hawkes and Mound*, 1984]. The shallower onlap horizon on SIGHT lines 25E and 2E coincides with a late Miocene (~11.5 Ma) horizon in both the Galleon-1 well (SIGHT line 25E) and the Clipper-1 well (SIGHT line 2E) (Figures 5b and 5c).

3.4. Industry Seismic Reflection Data

A comprehensive grid of industry seismic reflection data in the Canterbury Bight (light shaded region, Figure 1c) [*B.P. Shell Todd*, 1982; *Field and Browne*, 1989] also images the Oligocene horizon. All the lines that approach Dunedin show the Oligocene horizon to be uplifted (dark shaded region, Figure 1c) showing that it is a large-scale feature associated with Dunedin. A similar, but much smaller-scale uplift of the same horizon is seen on the parts of the lines that approach Banks Peninsula. Any uplift seen close to the southeast coast of South Island in the Canterbury basin is minor, suggesting that we are not just seeing relative uplift due to sediment loading in the Canterbury Bight but are seeing Miocene uplift somehow associated with the two major volcanic centers. The industry seismic data show no evidence for faulting being responsible for the steep uplift profile of the Oligocene and later horizons.

3.5. Helium Isotope Data

Radiogenic helium 4 (^{4}He) is generated by the radioactive decay of unstable isotopes of uranium and thorium and is present in relatively large quantities in the continental crust. Radiogenic helium 3 (primordial ^{3}He) is generated by the radioactive decay of lithium 6 (^{6}Li) and is generally present in small quantities in the continental crust. The average ratio of ^{3}He to ^{4}He in a sample (R), normalized by the ^{3}He/^{4}He ratio measured in air (R_a), R/R_a, is 0.005–0.02 for samples of continental crust [*Mamyrin and Tolstikhin*, 1984]. Significant

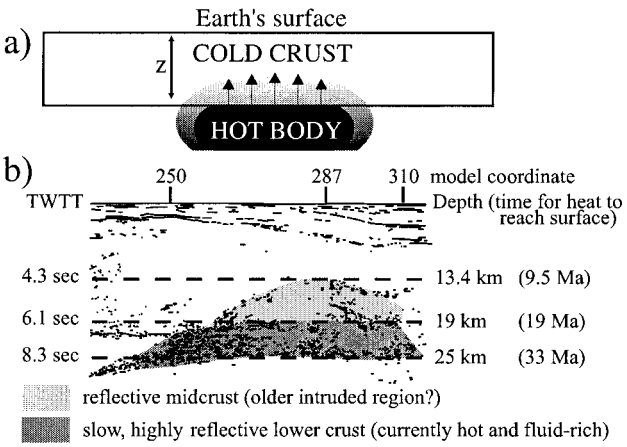

Figure 4. (a) Schematic for the vertical cooling of a hot body. The parameter z is the depth from the surface to the top of the cooling body. (b) Interpretation of multichannel seismic data showing the time calculated for heat to reach the surface. The calculation is done with the top of the heat source (dashed lines) at the Moho (~25 km), at the top of the low-velocity, highly reflective lower crust (~19 km) and at the top of the "normal velocity," reflective midcrust (4.3 s TWTT or ~13.4 km).

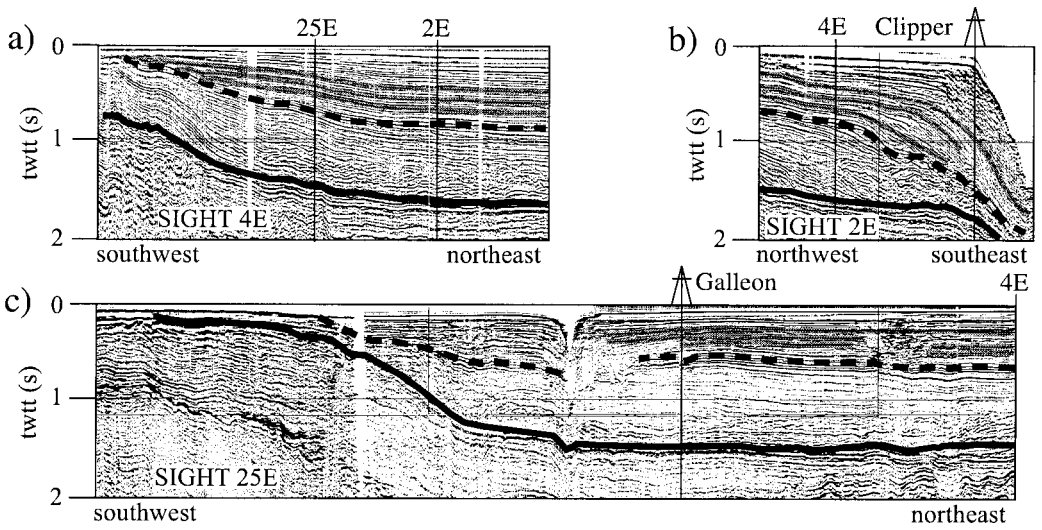

Figure 5. Top 2-s two-way travel time of data from three SIGHT multichannel seismic (MCS) lines. The locations of the lines are shown in Figure 1c. Vertical lines show well locations or the location of the intersection with a SIGHT MCS line. Bold solid line shows the Oligocene limestone horizon. Bold dashed line shows the late Miocene onlap horizon. Shaded lines show horizons that onlap onto the late Miocene horizon.

amounts of primordial ^{3}He in the continental crust define regions beneath which mantle melts exist and active basaltic addition to the crust is likely, since the mantle signature only remains in the crust for about 1–2 Myr [*O'Nions and Oxburgh*, 1983]. Helium isotopes can thus help differentiate between a radiogenically enriched upper mantle ($R/R_a < 8 \pm 1.5$), depleted upper mantle (mid-ocean ridge basalt (MORB), $R/R_a = 8 \pm 1.5$) and mantle plumes from the lower mantle ($R/R_a > 12$) [*Hoke et al*., 2000].

Helium ratios from the seven gas samples closest to Transect 3 show a range of R/R_a values between 0.38 and 6.97 [*Giggenbach et al*., 1993; *Hoke and Sutherland*, 1999; *Hoke et al*., 2000]. This gives mantle helium percentages of 4–88% [*Hoke et al*., 2000] (Figure 1b and Plate 1d), where the percentage is calculated from R/R_a of the sample divided by 8 (MORB). Values >10% are considered to show a significant mantle helium contribution [*Hoke et al*., 2000].

The helium isotope data from South Island suggest upper mantle melting beneath the volcanic centers, although the volcanic centers on South Island developed well away from the nearest subduction zone. There is also no evidence for significant crustal or lithospheric thinning which might have invoked mantle melting during the Miocene [*Hoke et al*., 2000]. No helium isotope ratios typical of the lower mantle associated with mantle plumes or hot spots have been recorded on South Island [*Giggenbach et al*., 1993; *Hoke and Sutherland*, 1999; *Hoke et al*., 2000]. Alkali basalts are restricted to the continental crust, and no hot spot traces related to these volcanic centers are observed on adjacent Pacific oceanic crust [*CANZ*, 1996; *Hoke et al*., 2000]. *Hoke et al*. [2000] suggested that the South Island volcanics are related to melting caused by thermal perturbations in the upper mantle, which may have remained attached to the continental plate since 40 Ma despite movement of the overlying Pacific plate.

Table 1. Industry Well Information[a]

	Clipper-1	Galleon-1
Drilled by	BP Shell Todd	Canterbury Services Ltd.
Year	1984	1985
Maximum depth, m	4742	3086
Closest MCS	2E	25E
Water depth, m	151	91
Seafloor TWTT, s	0.23	0.12
Pink horizon TWTT, s	1.498	0.782
Oligocene TWTT, s	1.732	1.472

[a]*Hawkes and Mound* [1984], *Wilson* [1985], and *Field and Browne* [1989].

3.6. Heat Flow Data

Background heat flow in the Great South basin, Southland basins (Figure 1b), and on the Western Platform of the Taranaki basin on North Island, all of which have a similar geological history, is ~60 mW m^{-2} [*Funnell et al*., 1996]. The heat flow data that we use (Figure 1b) are from *Funnell and Allis* [1996] and *Cook et al*. [1999]. The data are mostly from offshore industry wells, but there are four onshore sites in the database. The Canterbury basin, near the coast, shows slightly elevated heat flow values of 70–74 mW m^{-2}. The data from Macraes Flat mine near Dunedin, and a nearby offshore well, show extremely high heat flow (90–92 mW m^{-2}) (Figure 1b). The three onshore sites closest to the Banks Peninsula (Figure 1b) may be contaminated by cold deep groundwater, and the heat flow calculated at these sites may be an underestimate [*Funnell and Allis*, 1996; *Cook et al*., 1999]. There are no data from the Banks Peninsula itself.

There is a major heat flow anomaly in the Dunedin region, which persists northeast along the coast toward the Banks Peninsula. *Funnell and Allis* [1996] and *Cook et al*. [1999] attribute the high heat flow around Dunedin to anomalously high temperatures in the underlying lower crust and mantle associated with a thinned lithosphere. Simple 1-D models suggest the lithosphere may be as thin as 50 km in the Dunedin region compared with 100 km elsewhere beneath South Island [*Funnell and Allis*, 1996; *Cook et al*., 1999].

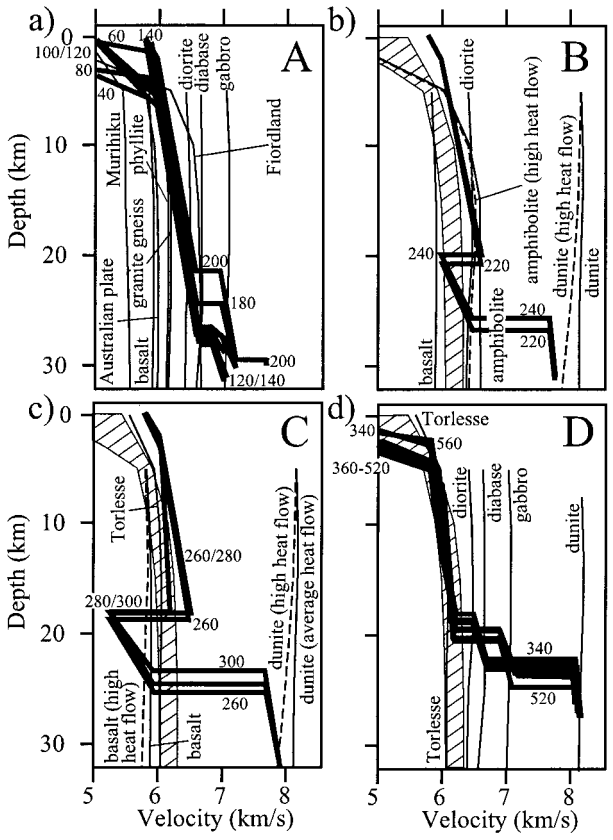

Figure 6. Velocity-depth profiles (bold lines) taken from the velocity model (see vertical arrows in Plate 1a). Numbers are the model coordinate of each profile. Each plot corresponds to a region shown in Plate 1a (see letters). Other profiles (solid lines for average heat flow and dashed lines for high heat flow) are for different lithologies (data taken from Table A1 and *Christensen and Mooney* [1995]). Regions marked with diagonal lines show the range of average velocities encompassed by Haast Schist (Table A1).

4. Interpretation and Further Modeling

4.1. Crustal Structure

4.1.1. Lithological interpretation of the velocity model. We extracted velocity-depth profiles from our velocity model and compared them with velocity-depth curves of various lithologies, including those represented at the surface, to interpret the lithology at depth beneath Transect 3 (see Appendix A and Figure 6).

The southwest part of the model (region A, model coordinates 0–210, Plate 1a and Figures 6a and 7), is consistent with mafic Median batholith and Brook Street terrane island arc dominating the crust. The Brook Street terrane is overlain by the very thin (based on our velocity model) Murihiku forearc basin (Figure 7a). This is the only part of the velocity model that is in possible conflict with surface geology. Laboratory-measured Murihiku terrane velocities are 4.8 km s^{-1} at sea level, 5.0 km s^{-1} at 2 km depth, and <5.5 km s^{-1} down to 15 km depth (Table A1 and Figure 6a). On the basis of velocity the Murihiku terrane appears to only be ~2 km thick, much thinner than expected, since the stratigraphic thickness of the Murihiku terrane is 10 km. *Pg* on gathers 5018 and 5019, however, is not consistent with velocities slower than the final model (Figure 2b and Plate 1a). We interpret the lower crust, which bows down with the Moho to form a root beneath the southwest end of Transect 3, as a 5-km-thick reflective gabbroic underplate (Plate 1a and Figures 6a and 7).

In regions B and C (model coordinates 220–320, Plate 1a), rocks with velocities faster than the measured values of Haast Schist are seen down to ~20 km depth (Figures 6b and 6c). We only have petrophysical measurements on Haast Schist samples that we believe were derived from Torlesse terrane graywackes. We expect Caples terrane graywackes to be more mafic, and faster, than Torlesse terrane graywackes. This suggests that Haast Schist in this region is derived from Caples terrane graywackes. The low-velocity regions of our velocity model (lower crust in region C and mantle in regions B and C, Plate 1a) were compared with candidate lithologies corrected for high heat flow (dashed lines, Figures 6b and 6c). The low-velocity lower crust in region C (Plate 1a), is slower than basalt corrected for high heat flow (Figure 6c). The presence of melt may lower the velocity further and we interpret the low-velocity lower crust as a hot, fluid-rich, possibly actively melting region. Dunite in a high heat flow setting is a suitable candidate for the low-velocity mantle in regions B and C (Figures 6b and 6c).

The northeast end of Transect 3 (region D, model coordinates 320–600, Plate 1a and Figures 6d and 7) can be interpreted as basin sediments overlying Torlesse graywacke, overlying Haast Schist derived from Torlesse graywacke down to 19–20 km depth at the top of the lower crust. The Caples/Torlesse boundary within the Haast Schist inferred from a change from faster velocities for the Caples-derived schist to slower velocities for the Torlesse-derived schist occurs at about model coordinate 290 (Figure 7). The lower crust is 5 km thick and is interpreted as mafic (diorite, diabase, and gabbro) Mesozoic(?) oceanic crust, presumably the crust on which the Torlesse accretionary prism accumulated (Figure 7). The Moho is fairly uniform in depth dipping slightly to the north east and overlies normal lithospheric mantle (Figure 7).

4.1.2. SIGHT MCS data. The highly reflective lower crust in the Dunedin region is coincident with the low-velocity lower crust of the velocity model (Plates 1a and 1c), and we interpret it as hot, fluid-rich basaltic crust.

4.2. Thermal History

4.2.1. Active melting. The strongest mantle helium anomaly on South Island (84–88%) is centered over Dunedin (Figure 1b and Plate 1d), suggesting that magmatic addition to the base of the crust is a recent event or even ongoing in this region, which contrasts with the volcanic history of the area. By comparison, samples from the Banks Peninsula have a much smaller, but still significant, mantle helium signature (25%, Figure 1b and Plate 1d). Mantle melting may be less active there.

4.2.2. Cooling rates. The heat flow measured at the surface today includes heat lost from a hot subsurface body sometime in the past. If there was an additional heat source within, or immediately below the crust, we can estimate the time taken for a heat pulse to reach the surface from various depths. For simplicity, we assume 1-D heat flow, that is, that no heat is lost laterally, no heat is lost from the base of the hot body, and all the heat is being lost through the crust to the surface.

For the 1-D case the time t taken for heat from the top of a hot body at depth z to reach the surface (Figure 4a) is given by *Sleep and Fujita* [1997]:

$$t = z^2 \rho c / k, \quad (1)$$

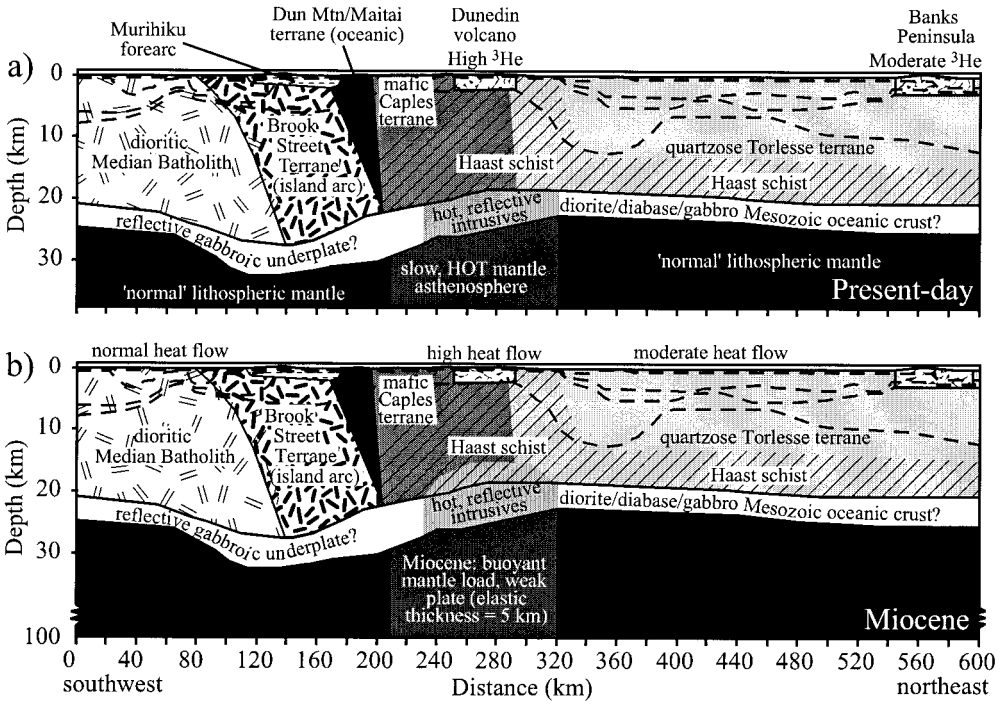

Figure 7. Schematic showing our interpretation of the geophysical data along Transect 3. (a) Interpretation of the present-day situation. (b) Interpretation of the Miocene situation.

where ρc is volume heat capacity (4×10^6 J m^{-3} K^{-1} for water and rocks) and k is thermal conductivity (2.4 W m^{-1} K^{-1} for granites and gabbros). This gives $t = z^2/18.9$, where z is in kilometers and t is in million years. We consider the following three cases.

4.2.2.1. Heat source entirely in the mantle immediately beneath the Moho: At model coordinate 287 (i.e., Dunedin) the Moho is at 25 km depth. Using $z = 25$ km gives $t = 33$ Ma (Figure 4b). Heat put into the system 33 Myr ago will only be appearing at the surface now. This does not fit with the main input of heat coinciding with peak volcanism at the Dunedin volcanic center during the Miocene (13–10 Ma).

4.2.2.2. Top of heat source at the top of the present-day lower crust: At model coordinate 287 the top of the lower crust (z) is at 19 km depth, which gives $t = 19$ Ma (Figure 5b). This means heat put into the system 19 Myr ago will only be appearing at the surface now. This fits better with the main input of heat coinciding with peak volcanism between 13 and 10 Ma but suggests that we are only seeing the start of the heat flow anomaly related to peak Miocene volcanism, with the highest heat flow anomaly to come in the future.

4.2.2.3. Top of heat source in the midcrust: There is a "dome" of reflectivity in the SIGHT MCS data (light shaded region, Figure 4b) that is shallower than the reflectivity associated with the top of the low velocity zone (dark shaded region, Figure 4b). This shallower reflectivity may represent older intrusions above the currently hot, fluid-rich region (dark shaded region, Figure 4b). The top of this dome of reflectivity at model coordinate 287 is at 4.3 s two-way travel time (13.4 km depth based on the velocity model). Using $z = 13.4$ km gives $t = 9.5$ Ma. This means that heat put into the system ~9.5 Myr ago will be appearing at the surface now. This fits better with the main input of heat coinciding with peak volcanism between 13 and 10 Ma and suggests we might be seeing the postpeak phase of the Miocene event.

The high heat flow in the Dunedin region can be explained as the peak, or postpeak, phase of the Miocene volcanic event, that is only now reaching the surface. Our simple calculation suggests that the heat source (region of melt) at the time the volcanic center was active in the Miocene was within the midcrust, shallower than suggested by the velocity model for the present day.

4.3. Flexural History

Well data show that the limestone horizon, which we have assumed was deposited flat and horizontally, was uplifted from the late Miocene, at around 11 Ma, and hence we make the important inference that the start of uplift was approximately coeval with the eruption of the Dunedin volcanics. We suggest a hot, buoyant load in the mantle beneath the volcanic centers may have been responsible for the uplift. We test this idea with a flexure model.

We have modeled the steep uplift profile of the Oligocene horizon near Dunedin (Figure 5) by invoking flexure of an elastic plate, with variable elastic thickness. Flexure is due to loading by a negative (buoyant) load beneath the Dunedin volcanic center and a positive load due to sediment addition in the Canterbury basin. The Oligocene limestone was deposited at ~0.2 km depth [*Field and Browne*, 1993] and is now at 1–1.5 km depth, except near Dunedin. The limestone horizon is at ~2 km depth around most of offshore New Zealand due to rapid subsidence in the last ~10 Myr [*Field and Browne*, 1993], although the reason for this rapid subsidence is uncertain.

We use a 2-D offshore model for simplicity (Figure 1a). The sediments extend into the Southern Alps toward the northwest and out to the edge of a deep basin to the southeast, and to a

first order a 2-D model is reasonable. Our results, however, show minimum load and maximum elastic thickness, since we believe the buoyant load is actually localized beneath the Dunedin volcanic center. Since we do not have the peak of the uplift profile beneath Dunedin (see truncated sediments in Figure 5a), the deflection we are fitting is a minimum, making our modeled load also a minimum.

For the sediment load in the Canterbury basin we use a rectangular load that has a thickness (0.5 km) equal to a water-filled basin that is equivalent, after subsidence, to a 1–1.5 km thick sediment-filled basin (Plate 1f). The present-day thickness of sediments above the late Miocene onlap horizon is based on a two-way travel time to the deepest part of the onlap horizon of 0.95 s and interval velocities of 2.2–3.15 km s^{-1} [*Stagpoole*, 1997]. The sediment load has a width equal to the length of the Canterbury basin.

In the Dunedin region we apply a 75-km-thick load (the distance between the approximately 25-km-deep Moho and the mantle lid at 100 km depth) (Plate 1e) whose magnitude and width are to be determined. This load represents asthenosphere replacing mantle and is therefore a density contrast with respect to normal mantle density.

The best fitting 2-D flexural model has a positive sediment load plus a 60-km-wide, negative (buoyant) load of 35 kg m^{-3} beneath Dunedin, with a weak elastic plate (5 km thick) beneath Dunedin (Plates 1e and 1g).

The steep profile of the data can not be modeled in two dimensions unless there is both a buoyant load in the mantle and a weak elastic plate beneath Dunedin (Figures 8a and 8b). Altering the magnitude of the load by as much as 5 kg m^{-3} makes the fit of the model to the data unacceptable (Figure 8c).

The change in mantle density (35 kg m^{-3}) represented by the load in the flexural model is related to a change in temperature of ~354°, assuming a thermal expansion coefficient of 3×10^{-5} K^{-1} [*Turcotte and Schubert*, 1982, p. 182]. This is consistent with temperatures predicted in the upper mantle from the high heat flow measured over Dunedin (~860° at 30 km depth) compared with the region outside Dunedin (~490° at 30 km depth) [*Funnell and Allis*, 1996; *Cook et al.*, 1999].

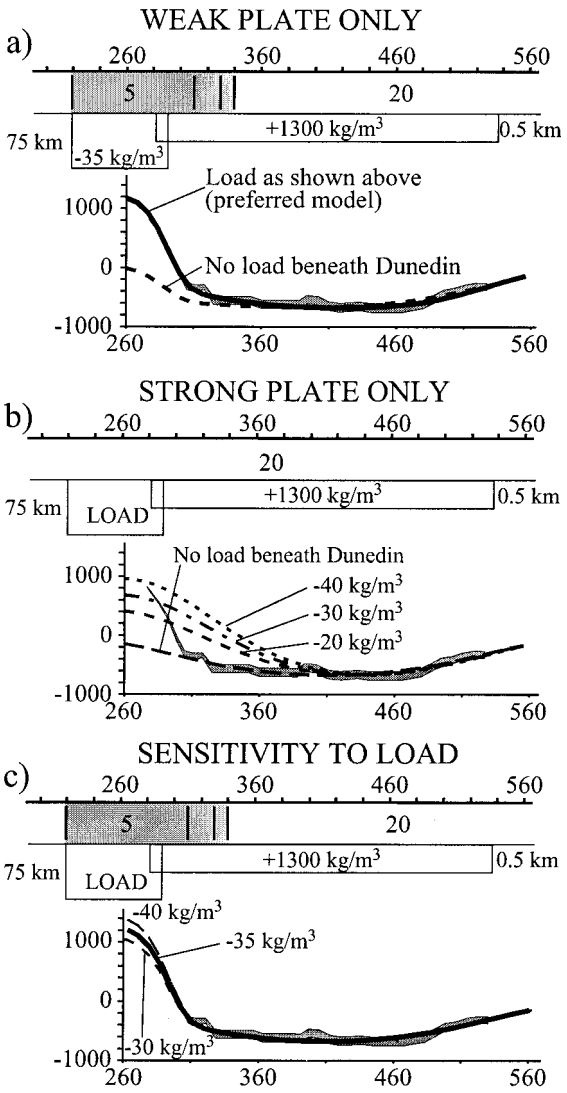

Figure 8. Tests on the flexural model. Model coordinates are shown along the top of the elastic thickness schematic and along the horizontal axis of the deflection plot and are the same as for Plate 1. For each part of the figure, the model and model parameters are shown at the top and the model fit (dashed or solid lines) to the data (shaded region) is shown below. For the model parameters the uppermost schematic shows elastic thickness (in km), with relatively low elastic thickness shown by shading. Underneath are shown the loads applied to each part of the model, with the thickness of each load (in km) shown to the side of the load. Restoring forces are the same as in Plate 1e.

5. Summary

We interpret all the geophysical anomalies associated with the Dunedin region (low-velocity mantle, extremely low velocity, highly reflective lower crust, high mantle helium ratios, a buoyant load in the mantle and weak elastic plate during the late Miocene, and high heat flow) as telling us about two thermal events associated with the Dunedin volcanic center. One event occurred during the Miocene, when volcanism was last actively occurring at the surface, and the other is occurring at present.

5.1. The Dunedin Volcanic Center

5.1.1. Present-day thermal event. The velocity model, MCS data, and helium isotope data tell us about present-day conditions in the crust and mantle. The low-velocity, highly reflective lower crust, which overlies low-velocity mantle, is probably due to the presence of hot, fluid-rich (melt?) material in the crust and mantle today (Figure 7a). High mantle helium ratios, which are most likely related to a current to recent (1–2 Ma) melting event in the mantle, support this idea. We interpret these data as showing a present-day thermal event associated with mantle and lower crustal melts beneath Dunedin and probable basaltic addition to the crust. Simple modeling of heat flow data suggest that heat from a hot body in the lower crust today will reach the surface in ~19 Ma. Volcanism associated with the present-day event has yet to reach the surface. The current compressive regime affecting South Island, which initiated with the change in plate motions at ~10 Ma, may make it difficult for magma associated with this event to reach the surface at all. *Watanabe et al.* [1999] suggest the initiation of the compressive regime may also have been responsible for shutting down the Dunedin volcano. If the melt formed due to thermal perturbations in the upper mantle, which has re-

mained attached to the continental plate over the last 40 Myr, as suggested by *Hoke et al*. [2000], we have no way of knowing the recurrence rate of volcanic activity at the Dunedin volcanic center. A present-day thermal event may be reasonable.

5.1.2. Miocene thermal event. The heat flow data reflect a thermal event some time in the past, since it takes a finite amount of time for heat emplaced in the crust or upper mantle to reach the surface. The present-day high heat flow can be explained by simple modeling as the thermal anomaly resulting from the peak or postpeak phase of the Miocene volcanic event, that is only now reaching the surface. During the Miocene the heat source (region of melt) was within the midcrust, shallower than suggested by the velocity model for the present-day thermal event. Flexural modeling suggests that the elastic thickness in the Dunedin region was small (5 km) implying a thermally weakened plate, and there was a buoyant load in the mantle, probably hot asthenosphere, which caused and maintained the uplift of sedimentary horizons in the Canterbury basin. The base of the midcrust is very reflective, but not as reflective as the lower crust. The midcrustal reflectivity may correspond to Miocene intrusives.

5.1.3. Alternative interpretation: A single thermal event. The WAR/R data reveal a low-velocity lower crust and upper mantle beneath Dunedin, which is most likely hot at present. The helium data suggest current or recent mantle melting but do not constrain the time at which this melting began. Volcanism and the flexural modeling presented in this paper suggest a thermal even during the Miocene, which may have continued as a single event to the present day. This is a feasible alternative interpretation given the uncertainty in the crust's thermal diffusivity.

5.2. Banks Peninsula Volcanic Center

During the Miocene the Banks Peninsula volcanic center was volumetrically more significant than the Dunedin volcanic center. The Banks Peninsula volcanic center may be expected to show similar features to the Dunedin volcanic center. Unfortunately, we do not have enough data to fully analyze this volcanic center. Mantle helium isotope percentages are elevated but not as high as in the Dunedin region. There are no heat flow data on the Banks Peninsula itself, and samples close to the Peninsula are most likely contaminated by cold groundwater [*Funnell and Allis*, 1996; *Cook et al*., 1999]. Our models do not extend far enough to the northeast to detect whether there are slow mantle velocities and highly reflective lower crust beneath the Banks Peninsula. We do see low-amplitude, south dipping reflectors on the northeasternmost part of SIGHT line 4E (Plate 1c), which may be related to intruded volcanics and/or zones of melt associated with the Banks Peninsula to the northeast.

Appendix A

A1. Summary of the Geology of the Eastern Province Terranes

The Eastern Province consists of the arc and forearc system of the New Zealand region (Figure 1a).

A1.1. Brook Street terrane. The Brook Street terrane is the remnant of a Permian volcano-plutonic arc. It consists of weakly metamorphosed volcanogenic sediments, basaltic-dacitic volcanics, and arc-root complexes of oceanic origin up to 16 km thick [*Coombs et al*., 1976].

A1.2. Murihiku terrane. The Murihiku terrane is a 10-km-thick sedimentary sequence that includes turbidite sequences and slope, shallow water deltaic, estuarine and terrestrial facies, all of which have been metamorphosed to zeolite facies [*Bishop and Turnbull*, 1996]. It is interpreted as a Triassic to Jurassic forearc basin [*Campbell and Coombs*, 1966; *Coombs et al*., 1976].

A1.3. Dun Mountain-Maitai terrane. The Dun Mountain-Maitai terrane includes the Dun Mountain ophiolite belt and the Maitai Group. It is in fault contact with both the Murihiku and Caples terranes [*Coombs et al*., 1976; *Mortimer*, 1993b]. The volcanic breccias, sandstones, mudstones, and limestones that make up the Permian to Triassic Maitai Group were derived from an inactive volcanic arc and deposited in a forearc or backarc setting. The Maitai Group overlies the Dun Mountain ophiolite belt (serpentinized harzburgite and dunite of oceanic affinity intercalated with Maitai Group rocks) along a local unconformity. The Dun Mountain ophiolite belt does not crop out at the surface at the coast and is assumed to lie at some depth beneath Transect 3.

A1.4. Caples terrane. The relatively mafic volcanoclastic Caples terrane, which is at least partly contemporaneous with the Torlesse terrane to the northeast, is more similar to the Brook Street terrane than the Torlesse terrane [*Norris and Craw*, 1987; *Mortimer*, 1993b]. It is interpreted as a forearc/trench accretionary complex [*Coombs et al*., 1976].

A1.5. Torlesse terrane. The Carboniferous-Permian to Jurassic Torlesse terrane consists of quartzo-feldspathic sandstones and graywackes [*MacKinnon*, 1983; *Norris and Craw*, 1987; *Mortimer*, 1993b]. The exact mode and location of its formation are uncertain [*Norris et al*., 1977; *Nur and Ben-Avraham*, 1977; *Kamp*, 1980; *MacKinnon*, 1983], although it is generally thought to represent an accretionary prism.

A2. Petrophysical Measurements Made on South Island Rocks

Laboratory measurements were made on samples from South Island collected as part of the SIGHT project (Table A1). Petrophysical measurements were made as described by *Godfrey et al*. [2000] and are reported here as the average compressional wave velocity measured through three mutually perpendicular cores taken from each sample [*Godfrey et al*., 2000]. The average velocities for all samples of a particular rock type at each pressure were averaged to give a single velocity value. Pressure was converted to depth and corrected for temperature (average heat flow and high heat flow) (Table A1) using the formulations given by *Christensen and Mooney* [1995], such that all velocity-depth curves shown in Figure 6 are comparable. High heat flow velocity values of *Christensen and Mooney* [1995] are based on Basin and Range temperature gradient, which is comparable to the elevated heat flow recorded on South Island [*Funnell and Allis*, 1996; *Cook et al*., 1999].

A3. Detailed Lithological Interpretation of the Transect 3 Velocity Model

We extracted velocity-depth profiles from our velocity model and compared them with velocity-depth curves of various lithologies to interpret the lithology at depth beneath Transect 3. Some of the velocity data (diorite, diabase, gabbro, basalt, phyllite, and dunite) are taken from *Christensen and Mooney* [1995]. All other velocity data are new laboratory velocity measurements made on samples from South Island.

Table A1. Compressional Wave Velocities and Densities of Samples Collected From South Island, New Zealand[a]

Depth, km	Velocity at Room Temperature, km s^{-1}	Velocity With Average Heat Flow, km s^{-1}	Velocity With High Heat Flow, km s^{-1}
	Haast Schist: Garnet-Oligoclase Zone		
	Density = 2707 kg m^{-3}		
0	4.478	4.478	4.478
10	6.006	5.943	5.900
20	6.175	6.051	5.975
30	6.267	6.081	5.953
	Haast Schist: Biotite Zone		
	Density = 2692 kg m^{-3}		
0	4.230	4.230	4.230
10	6.212	6.149	6.107
20	6.409	6.286	6.209
30	6.503	6.316	6.189
	Haast Schist: Chlorite IV Zone		
	Density = 2734 kg m^{-3}		
0	4.274	4.274	4.274
10	6.142	6.079	6.036
20	6.353	6.229	6.152
30	6.454	6.267	6.139
	Haast Schist: Chlorite III Zone		
	Density = 2738 kg m^{-3}		
0	4.957	4.957	4.957
10	6.246	6.183	6.141
20	6.436	6.313	6.236
30	6.529	6.342	6.215
	Haast Schist: Chlorite II Zone		
	Density = 2682 kg m^{-3}		
0	4.895	4.895	4.895
10	5.957	5.894	5.852
20	6.152	6.029	5.952
30	6.249	6.062	5.934
	Torlesse Terrane		
	Density = 2705 kg m^{-3}		
0	5.575	5.575	5.575
10	6.116	6.054	6.011
20	6.216	6.092	6.015
30	6.268	6.081	5.953
	Murihiku Terrane		
	Density = 2605 kg m^{-3}		
0	4.790	4.790	4.790
10	5.459	5.396	5.354
20	5.628	5.504	5.427
30	5.710	5.523	5.396
	Australian Plate		
	Density = 2653 kg m^{-3}		
0	4.986	4.986	4.986
10	5.977	5.916	5.874
20	6.103	5.983	5.908
30	6.165	5.983	5.858
	Fiordland		
	Density = 2866 kg m^{-3}		
0	4.073	4.073	4.073
10	6.577	6.516	6.475
20	6.758	6.638	6.563
30	6.835	6.653	6.529
	Amphibolite		
	Density = 2937 kg m^{-3}		
0	4.339	4.339	4.339
10	6.563	6.476	6.418
20	6.794	6.624	6.518
30	6.891	6.634	6.458

[a]Heat flow regimes are the same as in the study by *Christensen and Mooney* [1995].

A3.1. Region A (model coordinates 0–220). From southwest to northeast, the terranes exposed at the surface are the Median batholith, and the Brook Street, Murihiku, Maitai-Dun Mountain, and the Caples terranes (Plate 1b). Between 0 and 7 km depth modeled velocities are consistent with a wide range of lithologies (Figure 6a). Midcrustal velocities between 7 and 17 km depth are between those measured for diorite and basalt, both of which are consistent with crust composed of Median batholith, Brook Street terrane, or Maitai-Dun Mountain terrane rocks (Figure 6a). The velocities of the midcrust below 17 km depth are equivalent to those of diorite and diabase and consistent with either Median batholith or Brook Street terrane at the base of the midcrust. Below this, the 5- to 8-km-thick lower crust has velocities similar to gabbro (Figure 6a).

A3.2. Region B (model coordinates 220–250). Haast Schist, which is most likely derived from the relatively mafic Caples terrane graywackes in this region, is exposed at the surface in this region (Plate 1b). Caples terrane graywackes are expected to be more mafic and faster than Torlesse terrane graywackes. We only have petrophysical measurements on Haast Schist samples that we believe were derived from Torlesse terrane graywackes. Rocks with velocities faster than our measured values of Haast Schist are seen down to 14 km depth (Figure 6b). This suggests that Haast Schist in this region is derived from Caples terrane graywackes. The midcrust below 14 km depth has velocities consistent with diorite and amphibolite (Figure 6b), although this may also be fast Caples-derived schist. The 5- to 7-km-thick lower crust (20–27 km depth) is slightly faster than basalt but is consistent with Haast Schist or diorite in an average heat flow regime or amphibolite in a high heat flow regime (Figure 6b). The mantle is consistent with dunite in a high heat flow regime (Figure 6b).

A3.3. Region C (model coordinates 250–320). The geology exposed at the surface includes the Dunedin volcanic center (model coordinate 260–300) (Figure 3b). It is presumably underlain by Haast Schist.

Velocities above 9 km depth are fast compared to both our Haast Schist samples and basalt (Figure 6c, southwest of model coordinate 310). If the Haast Schist beneath the Dunedin volcanic center is derived from relatively mafic Caples terrane graywackes, rather than Torlesse graywackes, velocities may be faster than the measured Haast Schist values. Velocities between 9 and 18 km depth are consistent with, or faster than, measured values for Haast Schist (see profiles at model coordinates 260, 280, and 300, Figure 6c). This may indicate that between 9 and 18 km depth, the Torlesse-Caples boundary within the Haast Schist is between model coordinates 280 and 300. The 5- to 7-km-thick lower crust (18–25 km depth) has exceptionally low velocities, which are considerably slower than basalt in a high heat flow regime (Figure 6c). The relatively low velocity of the mantle is consistent with dunite in a high heat flow regime (Figure 6c).

A3.4. Region D (model coordinates 320–600). Torlesse graywacke is exposed onshore and is believed to continue offshore beneath the Canterbury basin and the Banks Peninsula volcanic center. Velocities in this region can be interpreted in terms of basin sediments overlying Torlesse graywacke, which in turn overlies Haast Schist down to 19–20 km depth at the base of the midcrust (Figure 6d). The 5-km-thick lower crust is consistent with diorite and diabase in the southwest half of region D and gabbro in the northeast half of region D (Figure

6d). Dunite in an average heat flow regime is consistent with mantle velocities in this region (Figure 6d).

Acknowledgments. The authors would like to thank David Okaya for initiating and organizing the collection of wide-angle reflection/refraction data along Transect 3 during the 1996 field season since it was not part of the original SIGHT proposal. We thank Nikolas Christensen for petrophysical data from South Island samples. N. J. Godfrey thanks Leonore Hoke, Robert Funnell and Nick Mortimer for helpful discussion while in New Zealand. The authors would also like to thank the Associate Editor and the reviewers, Kate Miller and John Townend, for helpful suggestions and comments. The work in this manuscript was funded by NSF grant EAR-9418530.

References

Allis, R. G., Continental underthrusting beneath the Southern Alps of New Zealand, *Geology*, *9*, 303–307, 1981.

Bishop, D. G., and I. M. Turnbull, Geology of the Dunedin area, *IGNS Geol. Map 21*, scale 1:250000, Inst. of Geol. and Nucl. Sci., Ltd., Lower Hutt, New Zealand, 1996.

Bishop, D. G., J. D. Bradshaw, and C. A. Landis, Provisional terrane map of South Island, New Zealand, in *Tectonostratigraphic Terranes of the Circum-Pacific Region*, edited by D. G. Howell, pp. 515–521, Circum-Pac. Counc. of Energy and Miner. Resour., Houston, Tex., 1985.

B.P. Shell Todd, Final operation report: Canterbury Bight petroleum prospecting licences 38202 and 38203, *Pet. Rep. 898*, 232 pp., Geol. Soc. of N. Z., Dunedin, 1982.

Campbell, J. D., and D. S. Coombs, Murihiku Supergroup (Triassic-Jurassic) of Southland and South Otago, *N. Z. J. Geol. Geophys*., *9*, 393–398, 1966.

Carter, R. M., and R. J. Norris, Cainozoic history of southern New Zealand: An accord between geological observations and plate tectonic predictions, *Earth Planet. Sci. Lett*., *31*, 85–94, 1976.

Charting Around New Zealand (CANZ), Undersea New Zealand (New Zealand region physiography), scale 1:4,000,000, N. Z. Oceanogr. Inst., Wellington, 1996.

Christensen, N. I., and W. D. Mooney, Seismic velocity structure and composition of the continental crust: A global review, *J. Geophys. Res*., *100*, 9761–9788, 1995.

Cook, R. A., R. Sutherland, and H. Zhu, Cretaceous-Cenozoic geology and petroleum systems of the Great South Basin, New Zealand, Inst. of Geol. and Nucl. Sci. Ltd., Lower Hutt, New Zealand, 1999.

Coombs, D. S., Dunedin Volcano, *Misc. Publ. 37B*, pp. 2–28, Geol. Soc. of N. Z., Dunedin, 1987.

Coombs, D. S., C. A. Landis, R. J. Norris, J. M. Sinton, D. J. Borns, and D. Craw, The Dun Mountain Ophiolite Belt, New Zealand, its tectonic setting, constitution, and origin, with special reference to the southern portion, *Am. J. Sci*., *276*, 561–603, 1976.

Coombs, D. S., R. A. Cas, Y. Kawachi, C. A. Landis, W. F. McDonough, and A. Reay, Cenozoic volcanism in north, east and central Otago, *Bull. R. Soc. N. Z*., *23*, 278–312, 1986.

Cooper, A. F., B. A. Barreiro, D. L. Kimbrough, and J. M. Mattinson, Lamprophyre dyke intrusion and the age of the Alpine fault, New Zealand, *Geology*, *15*, 941–944, 1987.

Davey, F. J., et al., Preliminary results from a geophysical study across a modern continent-continent collisional plate boundary—the Southern Alps, New Zealand, *Tectonophysics*, *288*, 221–235, 1998.

Duggan, M. B., and A. Reay, The Timaru basalt, *Bull. R. Soc. N. Z*., *23*, 264–277, 1986.

Field, B. D., and G. H. Browne, Cretaceous and Cenozoic sedimentary basins and geological evolution of the Canterbury region, South Island, New Zealand, report, 170 pp., N. Z. Geol. Surv., Geophys. Div., Lower Hutt, 1989.

Field, B. D., and G. H. Browne, A subsiding platform adjacent to a plate boundary transpression zone: Neogene of Canterbury, New Zealand, in *South Pacific Sedimentary Basins*, edited by P. F. Ballance, pp. 271–278, Elsevier Sci., New York, 1993.

Funnell, R. H., and R. G. Allis, Hydrocarbon maturation potential of offshore canterbury and Great South Basins, paper presented at 1996 New Zealand Petroleum Conference, Publicity Unit, N. Z. Crown Miner., Minist. of Commer., Wellington, 1996.

Funnell, R. H., D. S. Chapman, R. G. Allis, and P. A. Armstrong, Thermal state of the Taranaki basin, New Zealand, *J. Geophys. Res*., *101*, 25,197–25,215, 1996.

Gibson, G. M., and T. R. Ireland, Granulite formation during continental extension in Fiordland, New Zealand, *Nature*, *375*, 479–482, 1995.

Giggenbach, W. F., Y. Sano, and H. Wakita, Isotopic composition of helium, and CO_2 and CH_4 contents in gases produced along the New Zealand part of a convergent plate boundary, *Geochim. Cosmochim. Acta*, *57*, 3427–3455, 1993.

Godfrey, N. J., N. I. Christensen, and D. A. Okaya, Anisotropy of schists: Contribution of crustal anisotropy to active-source seismic experiments and shear wave splitting observations, *J. Geophys. Res*., *105*, 27,991–28,007, 2000.

Hawkes, P. W., and D. G. Mound, Clipper-1 geological completion report, *Pet. Rep. 1036*, 546 pp., N. Z. Geol. Surv., Lower Hutt, 1984.

Hoke, L., and R. Sutherland, The mantle beneath mainland New Zealand constrained by helium isotopes, map, scale 1:2,000,000, Inst. of Geol. and Nucl. Sci. Ltd., Lower Hutt, New Zealand, 1999.

Hoke, L., R. Poreda, A. Reay, and S. D. Weaver, The subcontinental mantle beneath southern New Zealand, characterised by helium isotopes in intraplate basalts and gas-rich springs, *Geochim. Cosmochim. Acta*, *64*, 2489–2507, 2000.

Holt, W. E., and T. A. Stern, Subduction, platform subsidence and foreland thrust loading: The late Tertiary development of Taranaki Basin, *N. Z. Tectonics*, *13*, 1068–1092, 1994.

Kamp, P. J. J., Pacifica and New Zealand: Proposed eastern elements in Gondwanaland's history, *Nature*, *288*, 659–664, 1980.

MacKinnon, T. C., Origin of the Torlesse terrane and coeval rocks, South Island, New Zealand, *Geol. Soc. Am. Bull*., *94*, 967–985, 1983.

Mamyrin, B. A., and I. N. Tolstikhin, *Helium Isotopes in Nature*, 273 pp., Elsevier Sci., New York, 1984.

Molnar, P., T. Atwater, J. Mammerickx, and S. M. Smith, Magnetic anomalies, bathymetry and the tectonic evolution of the South Pacific since the Late Cretaceous, *Geophys. J. R. Astron. Soc*., *40*, 383–420, 1975.

Mortimer, N., Jurassic tectonic history of the Otago Schist, New Zealand, *Tectonics*, *12*, 237–244, 1993a.

Mortimer, N., Geology of the Otago Schist and adjacent rocks, *IGNS Geol. Map 7*, scale 1:500000, Inst. of Geol. and Nucl. Sci. Ltd., Lower Hutt, New Zealand, 1993b.

Mortimer, N., A. J. Tulloch, R. N. Spark, N. W. Walker, E. Ladley, A. Allibone, and D. L. Kimbrough, Overview of the Median Batholith, New Zealand: A new interpretation of the geology of the Median Tectonic Zone and adjacent rocks, *J. Afr. Earth Sci*., *29*, 257–268, 1999.

Norris, R. J., and D. Craw, Aspiring Terrane: An oceanic assemblage from New Zealand and its implications for terrane accretion in the Southwest Pacific, in *Terrane Accretion and Orogenic Belts*, *Geodyn. Ser*., vol. 19, edited by E. C. Leitch and E. Scheibner, pp. 169–177, AGU, Washington, D. C., 1987.

Norris, R. J., C. A. Landis, and C. M. Ward, The relationship of the Rangitata orogen to possible plate configurations in the south Pacific (abstract), *Geol. Soc. N. Z. Annu. Conf*., *22A*, 41, 1977.

Norris, R. J., P. O. Koons, and A. F. Cooper, The obliquely-convergent plate boundary in the South Island of New Zealand: Implications for ancient collision zones, *J. Struct. Geol*., *12*, 715–725, 1990.

Nur, A., and Z. Ben-Avraham, Lost Pacifica continent, *Nature*, *270*, 41–43, 1977.

O'Nions, R. K., and E. R. Oxburgh, Heat and helium in the Earth, *Nature*, *306*, 429–431, 1983.

Rattenbury, M. S., Timing of mylonitisation west of the Alpine fault, central Westland, New Zealand, *N. Z. J. Geol. Geophys*., *30*, 287–297, 1987.

Reilly, W. I., Gravitational expression of the Dunedin volcano, *N. Z. J. Geol. Geophys*., *15*, 16–21, 1972.

Sleep, N. H., and K. Fujita, *Principles of Geophysics*, 586 pp., Blackwell Sci., Malden, Mass., 1997.

Stagpoole, V., A geophysical study of the northern Taranaki basin, New Zealand, Ph.D. thesis, 245 pp., Victoria Univ. of Wellington, Wellington, New Zealand, 1997.

Stern, T. A., and U. S. ten Brink, Flexural uplift of the Transantarctic Mountains, *J. Geophys. Res*., *94*, 10,315–10,330, 1989.

Stern, T. A., P. E. Wannamaker, D. Eberhart-Phillips, D. Okaya, F. J. Davey, and S. I. P. W. Group, Mountain building and active deformation studied in New Zealand, *Eos Trans. AGU*, *78*, 329, 335–336, 1997.

Turcotte, D. L., and G. Schubert, *Geodynamics*, John Wiley, New York, 1982.
Walcott, R. I., Plate motion and shear strain rates in the vicinity of the Southern Alps, *Bull. R. Soc. N. Z.*, *18*, 5–12, 1979.
Walcott, R. I., Reconstruction of the New Zealand region for the Neogene, *Paleogeogr. Paleoclimatol. Paleoecol.*, *46*, 217–231, 1984.
Walcott, R. I., Modes of oblique compression: late Cenozoic tectonics of the South Island of New Zealand, *Rev. Geophys.*, *36*, 1–26, 1998.
Watanabe, T., et al., Tectonic stress controls on ascent and emplacement of magma, *J. Volcanol. Geotherm. Res.*, *91*, 65–78, 1999.
Watson, S., and D. McKenzie, Melt generation by plumes: A study of Hawaiian volcanism, *J. Petrol.*, *32*, 501–537, 1991.
Wilson, I. R., Galleon-1 geological completion report, *Pet. Rep. 1146*, 1108 pp., N. Z. Geol. Surv., Lower Hutt, 1985.
Wood, R., and R. Sutherland, Reconstructing the southwest Pacific, *Eos Trans. AGU*, *78*, 21–22, 1997.

F. Davey, Institute of Geological and Nuclear Sciences, P.O. Box 30368, Lower Hutt, New Zealand. (f.davey@gns.cri.nz)
N. J. Godfrey, Landmark EAME, 203 Brooklands Road, Weybridge, Surrey KT13 0RH, England, UK. (ngodFrey@lgc.com)
D. Okaya, Department of Earth Sciences, University of Southern California, University Park, Los Angeles, CA 90089-0740, USA. (okaya@usc.edu)
T. A. Stern, Research School of Earth Sciences, P.O. Box 600, Victoria University, Wellington, New Zealand. (tim.stern@vuw.ac.nz)

(Received October 10, 2000; revised June 15, 2001;
accepted June 25, 2001.)